Perfluoropolyether-Based Micellar Aggregates Coatings for Corrosion Resistance Enhancement of Copper-Based Alloys

(Article begins on next page)

23 April 2024

alloys

MDPI

Article

Perfluoropolyether-Based Micellar Aggregates Coatings for Corrosion Resistance Enhancement of Copper-Based Alloys

Emilio Bassini [1,*] , **Federico Simone Gobber** [1] , **Elisa Fracchia** [2] , **Chiara Zenaro** [3] **and Enrico Boccaleri** [4]

1 Dipartimento di Scienza Applicata e Tecnologia (DISAT) Corso Duca degli Abruzzi, Politecnico di Torino, 24 10129 Torino, Italy
2 Dipartimento di Gestione Produzione e Design (DIGEP) Corso Duca degli Abruzzi, Politecnico di Torino, 24 10129 Torino, Italy
3 Dipartimento di Scienze e Innovazione Tecnologica via Teresa Michel, Università del Piemonte Orientale Amedeo Avogadro, 11 15121 Alessandria, Italy
4 Dipartimento per lo Sviluppo Sostenibile e la Transizione Ecologica (DiSSTE), Università del Piemonte Orientale Amedeo Avogadro, Piazza S. Eusebio, 5 13100 Vercell, Italy
* Correspondence: emilio.bassini@polito.it; Tel.: +39-0131-229352

Abstract: In this paper, a perfluoropolyether (PFPE) micellar solution was effectively deposited on metallic substrates using a dip-coating process to enhance brass and nickel aluminum bronze (NAB) corrosion resistance. Particular attention was paid to the aesthetic results as well. Enabling the metallic substrates hydrophobic to facilitate water and moisture removal was the key concept of this work. The corrosion resistance of the as-received and coated metals was investigated via a salt spray chamber test. The study focused on the characterization of the polymeric coating via dynamic light scattering and wettability tests, while the substrates were assessed with traditional metallographic techniques. The preparation of the polymeric solution was important in determining the final corrosion resistance of the two substrates. Noteworthy was the effectiveness of the PFPE-based coating when it was applied to the brass rather than the NAB. Moreover, the polymer concentration of the dip-coating polymeric emulsion was the most significant factor to obtaining adequate protection: higher polymer concentrations resulted in a decrease in corrosion resistance.

Keywords: corrosion resistance; nickel aluminum bronze (NAB); α + β brass; PFPE micelle; dip-coating

1. Introduction

This research work aims to prove the feasibility of applying perfluoropolyether-based coatings for preventing the corrosion of copper-based alloys—specifically, a nickel aluminum bronze (NAB) and an α + β brass.

Polymeric coatings are typically used to protect metallic materials with low corrosion resistance, with paintings being the most common. In this paper, PFPE polymers were chosen because of their ability to alter surface wettability.

These polymers are synthesized via the UV-radical polymerization of tetrafluoroethylene and hexafluoropropylene monomers mixture in low-temperature reactors containing oxygen. Once these polymers are fully fluorinated, they closely resemble fluorocarbons with good chemical, thermal, and biological inertia and high gas permeability. These properties directly correlate to the C-F and C-O presence along the polymer chains [1,2].

PFPE can be used in different formulations to obtain microemulsions by mixing them in water-oil (w/o) or water-oil-alcohol (w/o/a) systems working as anionic surfactants. More specifically, surfactant micelles are likely to form when these polymers are dispersed in systems containing short-chain oils and long-chain alcohols. On the other hand, long-chain oils with short-chain alcohols inhibit micelle formation [3,4].

PFPEs' chemical and physical properties allow their application in several fields, such as electronics and lubrication. Lately, they have been used as coatings for carbon nanotubes, permeable gas membranes, and silicon-based hierarchical materials. In all these cases, applying the PFPE reduced the wettability of the modified surfaces largely, making them superhydrophobic [5–10].

The materials studied in this paper are already corrosion-resistant, especially when environmental conditions are mild. When higher corrosion resistance is needed, as in power plant production or gas turbine, Nickel-based alloys are commonly adopted, as can be read in the work of Marchese [11] and Bassini [12].

Copper and brass corrosion resistance are closely related to the formation of a passivating layer on their surface. More specifically, brass typically corrodes due to a dezincification process. First, dezincification is an electrochemically activated process characterized by the selective dissolution of zinc from the surface layer. Secondly, copper is dissolved and deposits onto the surface, forming a discontinuity that can be easily detected due to its reddish color. This phenomenon is typical for non-homogenized $\alpha + \beta$ brasses with a Zn content higher than 15% and occurs in phases with a higher Zn content, i.e., the β one [13]. Finally, the presence of Cl ions (as in the salt spray chamber) is likely to increase the speed of the entire process, leading to complex copper-based compounds [14,15].

On the other hand, NAB corrosion is more complex and typically starts in the eutectoid regions. Here, the contemporary presence of α (anodic) and k3 (cathodic) phases makes these regions easily corrodible in the presence of an electrolyte. On the other hand, the α phase on its own has good corrosion resistance. Finally, retained β' phase, if present, could be easily corroded [16]. Nevertheless, when the NAB microstructure is optimized (after tailored heat treatment), the overall corrosion resistance of these alloys is quite good, thanks to the presence of a thin superficial passivating layer (900–1000 nm in thickness). This layer is formed thanks to the copper anodic reaction when Cl^- ions are also involved. As a result, the $CuCl^{2-}$ concentration increases up to its saturation limit and begins to precipitate as CuCl, which is likely to react with oxygen, forming a stable Cu_2O oxide. This reaction typically occurs in the α phase, where copper concentration is higher. This process locally consumes Cu, increasing the concentration of Al in the corroded grains. Once the Al content is high enough to promote the formation of alumina oxide, this phase starts to form, leading to a dual-layer oxide. The resulting oxide layer is richer in Cu at the surface, while a higher Al content is found below. At the same time, $Cu_2(OH)_3Cl$ or $Cu(OH)Cl$ compounds are likely to form due to the complexity of NAB systems [13,16–18]. Due to their high corrosion resistance, the coated materials were tested within a salt spray chamber to simulate more severe conditions expected in a marine environment for a long exposure time.

Applying a hydrophobic coating further helps the material to withstand corrosion resistance, avoiding moisture from damaging the passivating layer. This type of approach is currently studied and applied in a variety of fields.

This technique was efficiently applied to other metals such as zinc for the construction of batteries with better performances. In the work of Tao, PFPE limits H_2O exposure on the Zn surface, extending its life. Moreover, an in situ ZnF_2 layer also forms, providing further protection from corrosion [19]. The application of a hydrophobic polymeric layer on a mixed metal surface is acquiring great interest in the battery production field in particular. Schroder et al., for example, efficiently applied an ultrathin PV_3D_3 layer with fluorine functionality to protect metal oxide-based gas sensors from moisture [20]. Similar approaches were used also on different metals, such as lithium, to protect the metals in harsh environments with a high humidity content [21]. This time, a complex polymer containing lithium and fluorine was used for enhancing the properties of batteries for high energy storage systems. Nevertheless, all these techniques require complex deposition systems. Conversely, this study shows an easy and environmentally friendly approach for metal protection against moisture. This preliminary study involves copper-based alloys,

but the promising results obtained could set the basis for this coating to be applied to a wider set of alloys, such as iron or aluminum-based materials, as also proposed by [22].

Water dispersed perfluoropolyethers (PFPE) with low molecular weight and different concentrations were spread onto the copper-based metallic surfaces, making them hydrophobic, thus, limiting the interactions between water drops and the metallic surface.

According to the literature, PFPE is usually adopted to modify the superficial behavior of carbon-based [23] or silica-based-hierarchical materials [24]. However, this type of polymer is widely used as a lubricant when metals are concerned, as proposed by Lin et al. [25]. Still, no literature work has been found related to enhancing the corrosion resistance of copper-based alloys. A similar technique was used by Zhang et al., but in that case, tests were performed on aluminum-based material [26]. This paper aims to fill this gap, focusing on how the polymer concentration and deposition technique modify the final material behavior.

It is noteworthy to underline that this work focuses on the esthetical properties of the material, aiming to maintain the surface finishing as long as possible, while mechanical degradation was neglected.

The final aim is to optimize the layer composition to maximize the corrosion resistance without impairing the metal surface appearance, especially when artistic goods or architectural assets are concerned.

2. Materials and Methods

2.1. PTFE Solutions for Dip-Coating

As mentioned above, the protective layer is a commercial product, perfluoropolyether-based, with an initial concentration of 5% vol in water. The emulsion contains bifunctional linear chains with a molecular weight ranging between 1300 and 2000 and a density equal to 1.8 g/cm^3 at 20 °C. This polymer is stable up to 250 °C [27]. The commercial product was diluted to obtain 1 and 3% vol concentrations. These two emulsions are referred to as PFPE 1% and PFPE 3%. The emulsions were obtained by continuous stirring in demineralized water. The pH was maintained at a constant of 8.5 by adding NH_3 to the emulsion.

The water-based emulsion was deposited onto metallic surfaces using the dip-coating technique. The sample immersion into the solution was guaranteed by a motorized slider capable of moving at 1mm/s.

The two emulsions were assessed with dynamic light scattering equipment to measure the size of the micelles, which resulted as being slightly dependent on the dilution. The PFPE 1% and PFPE 3% contained micelles of 26.7 ± 7.3 nm and 31.6 ± 8.2 nm in size, respectively.

2.2. Metallic Substrates

The emulsions were deposited onto two metallic substrates, brass and a NAB. The brass used in this work was an α + β alloy whose composition, obtained via energy dispersive spectroscopy (EDS), is reported in Table 1. The brass alloy was cast using a low-pressure induction casting machine TVC-d by Topcast. The inductor was set at 12 kW, and the melt temperature was 1100 °C; 350 g of material was cast into a cylindric mold. The ingot was then homogenized at 800 °C for 1 h. Finally, the bar was cut into 10 discs with a 26 mm diameter and 6 mm thickness. A hole was drilled to connect the discs to the motorized slit used for the dip-coating. The material hardness was 96 ± 3 HBW 5, measured with a universal hardness machine by EMCO-TEST using 31.5 kg and a 2.5 mm sphere.

Table 1. Brass chemical composition as per EDS spectroscopy.

Elements	Cu	Zn	O	Pb
w%	57.34	29.68	8.04	3.82
Dev. St.	1.17	0.98	0.79	1.02

The NAB was tested in the as-received conditions without applying any heat treatment. The wrought material was cut to obtain discs with the exact shape of the brass ones. Moreover, in this case, a hole was drilled to simplify the dip-coating process. The material hardness was higher, i.e., 212HBW 5. The chemical composition obtained via EDS is shown in Table 2.

Table 2. NAB chemical composition as per EDS spectroscopy.

Elements	Cu	Al	Fe	Ni	Si
w%	73.07	18.79	4.15	1.23	0.76
Dev. St.	0.63	0.48	0.32	0.32	0.28

2.3. Dip-Coating Process

The samples were ground with SiC papers down to 1200 grits and polished with diamond pastes down to 1 μm. The final finishing was obtained by polishing with colloidal silica for 180 s. The samples were mirror polished to neglect any possible interaction effect of roughness and evaluate the adhesion of the coating in such a limiting condition. The roughness of the two materials was assessed with a Hommelwerke T1000 profilometer. Each sample was tested three times in different positions using a cut-off length of 0.25 mm and a measuring distance of 25 mm. The probe had a 0.5 mm/s speed. The final Ra average values are 0.042 ± 0.02 and 0.024 ± 0.01 μm for the brass and the NAB, respectively.

The brass or NAB discs were accurately cleaned with acetone within an ultrasonic bath before dipping them in the abovementioned solutions. Next, the discs were connected to the motorized slider using a fluorocarbon wire passing through the 4 mm hole. The two solutions were continuously mixed using a magnetic stirrer. Discs were submerged into the micro-emulsions for 10 min and then extracted in a controlled manner with a fixed speed of 1 mm/s to ensure a homogeneous deposition of the coatings. Finally, the coated discs were air-dried until all the solvent evaporated. This technique allowed the formation of a continuous layer onto the substrates, whose thickness is reported in Table 3.

Table 3. Average thickness of coatings obtained after dip-coating on Brass and NAB.

	Brass		NAB	
	PFPE 1%	**PFPE 3%**	**PFPE 1%**	**PFPE 3%**
Average layer thickness [μm]	0.85	0.91	0.78	0.94
Deviation from average [μm]	0.11	0.23	0.24	0.29

2.4. Waterdrop Contact Angle (CA) Assessment to Estimate the Surface Hydrophobicity

The wettability of uncoated and coated substrates was measured to assess the deposition effectiveness and the homogeneity of the deposited layers. Surface wettability was measured with a sessile drop tensiometer at five different points. The water drop was released onto the investigated surface, the dropout was 3 μm, and the contact angle was measured with a camera for 10 s at 12 fps. The image processing software measures both left and right contact angles and averages the two. The measured angle after 5 s was used for comparison across the samples. On the other hand, the complete plot of the CA was used to assess the stability of the coating, as also proposed by Bracco et al. [28].

2.5. Sample Preparation and Salt Spray Chamber Test

The salt spray test was conducted on as-polished and coated samples to compare the corrosion resistance of the materials thoroughly. Tests were performed following ISO 9227-2017 standard; the chamber and vapor temperatures were 35 °C and 49 °C, respectively. The salt spray solution contained 5% NaCl; the samples were hung vertically and inspected after 1, 2, 6, 8, 24, and 48 h.

2.6. Metallographic Preparation

The sample microstructure was revealed using different etching techniques, depending on the specific aim of the investigation. The general brass structure was evidenced using Klemm-colored etching. This reagent is prepared by mixing 20 g of $Na_2S_2O_3$ in 50 mL of deionized water. This solution must be prepared on a heated plate to avoid the precipitation of crystals due to oversaturation. Then, 1 g of $K_2S_2O_3$ is added to the water-based solution. The etching lasts between 120 and 180 s. Alternatively, finer details were revealed with ASTM 30 etching, consisting of 25 mL of NH_4OH mixed in a solvent of 25 mL of water and 50 mL of H_2O_2. The etching should not last more than 15–20 s. The investigations were performed with optical and electronic microscopy using a Leica MEF4 and a Leo 1430 VP, respectively. The corrosion products were assessed with EDS spectroscopy using an Oxford Instruments probe model 6587 Link Pentafet.

3. Results

3.1. Core Microstructure of Metallic Substrates

The Klemm etchant selectively bonds to the brass β phase, and light interacts differently depending on the thickness of the salt layer bonded to the material, therefore, resulting in different colors when the sample is observed under polarized light (see Figure 1) [29]. The acicular α phase, on the other hand, does not react with the reagent and, thus, remains white. The samples etched with the ASTM solution and observed with SEM show similar features. Nonetheless, the higher magnification allows the appreciation of the lead particles dispersed within the matrix (white particles), enhancing the alloy's machinability [30].
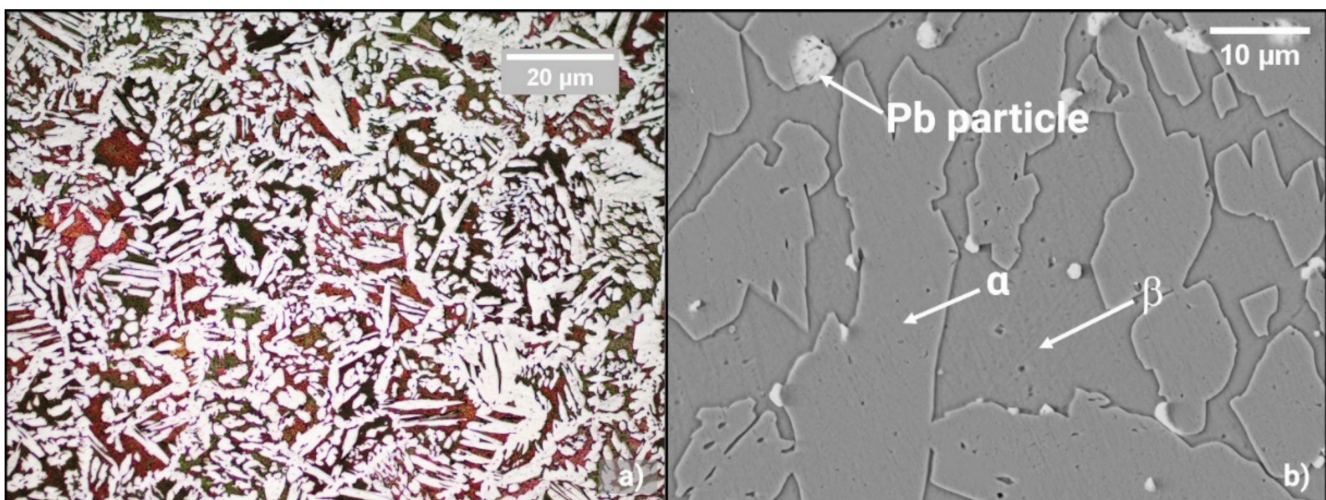

Figure 1. Brass microstructure observed with an optical microscope and polarized light (**a**) and with SEM using backscattered electrons detector (**b**).

As shown in Figure 2, the NAB microstructure appears much more complex and varied due to several Fe-based intermetallics (k1, k2, k3, and k4) [31]. Brighter phases within the grains, with Witmanstätten shape, is the α phase, while the surrounding is occupied by β with a higher Al-content. K phases can be divided into different categories based on their shape and precipitation site. K1 precipitates within the α phase and can be reported as Fe_3Al, but its formation requires an iron content higher than 5% and Ni lower than 0.5%. K2 can be easily recognized because of its rosette-like shape, and it forms within β grains [32]. K2 shares the chemical formulation with k1. K3 is a mixture of two intermetallics, i.e., NiAl + FeAl, and derives from the decomposition of β after a eutectoidic reaction (β→α + k3) [33].
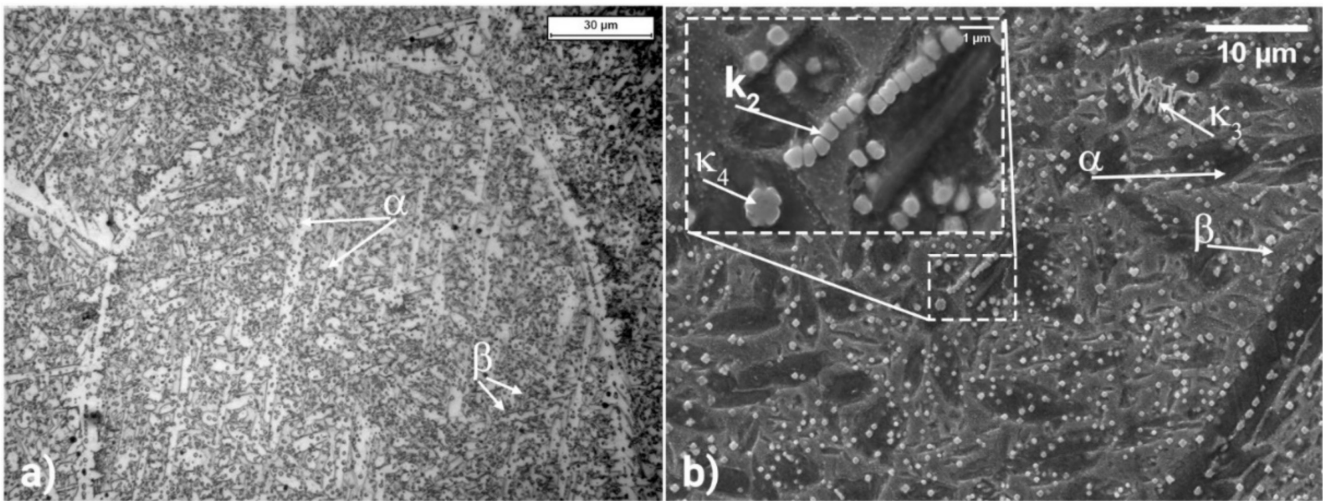
Figure 2. NAB microstructure observed with an optical microscope (**a**) and with the SEM (**b**) the inset shows the finer intermetallics.

As a consequence of the eutectoidic reaction, this phase has a typical lamellar aspect. Finally, k4 is like k2, but it precipitates in α grains. All these phases and intermetallics are identified in the SEM figures. The optical micrographs were used to assess the grain size, ranging between 1 and 2 ASTM standard values.

3.2. Surface Wettability and Contact Angle Assessment

After coating the Cu-based alloys, the contact angle was used to score the hydrophobicity level. The uncoated brass and NAB surfaces show similar hydrophilic behavior, as shown in Figure 3, for the as-received condition. The two contact angles are very close, and these minor differences may be ascribed to the surface roughness and the chemical composition.
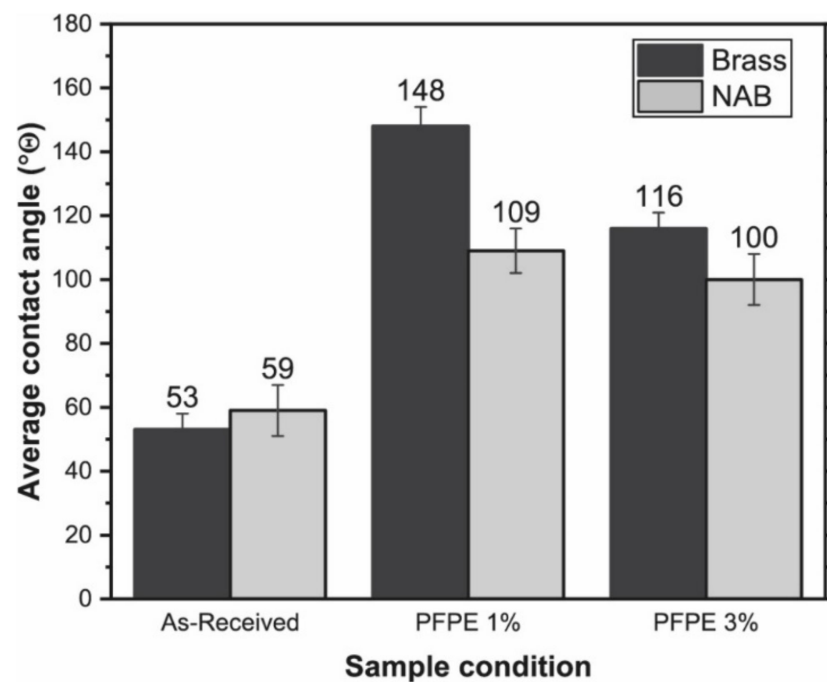

Figure 3. Contact angle of water drop on metallic substrates before and after the dip-coating. When higher polymer concentrations are used, the contact angle decreases.

The application of the polymeric coating significantly contributes to making the surfaces hydrophobic. It is worth noting that the results are considerably better when the brass is coated. Secondly, as the polymer concentration in the coating emulsion increases, the overall hydrophobic effects decrease. This effect is particularly evident for the brass alloy, while the NAB is slightly affected. Nevertheless, according to this preliminary test, the coating on the NAB could be less effective in preventing corrosion during the salt spray test.

The contact angles shown above were measured after the waterdrop stabilized onto the metal surface. The stability of the coating was investigated by observing the variability of the drop during the entire recording time window of the instrument, i.e., 10 s. Figure 4 shows the deviation from the initial contact angle for the brass and the NAB, respectively, with all the investigated coatings.
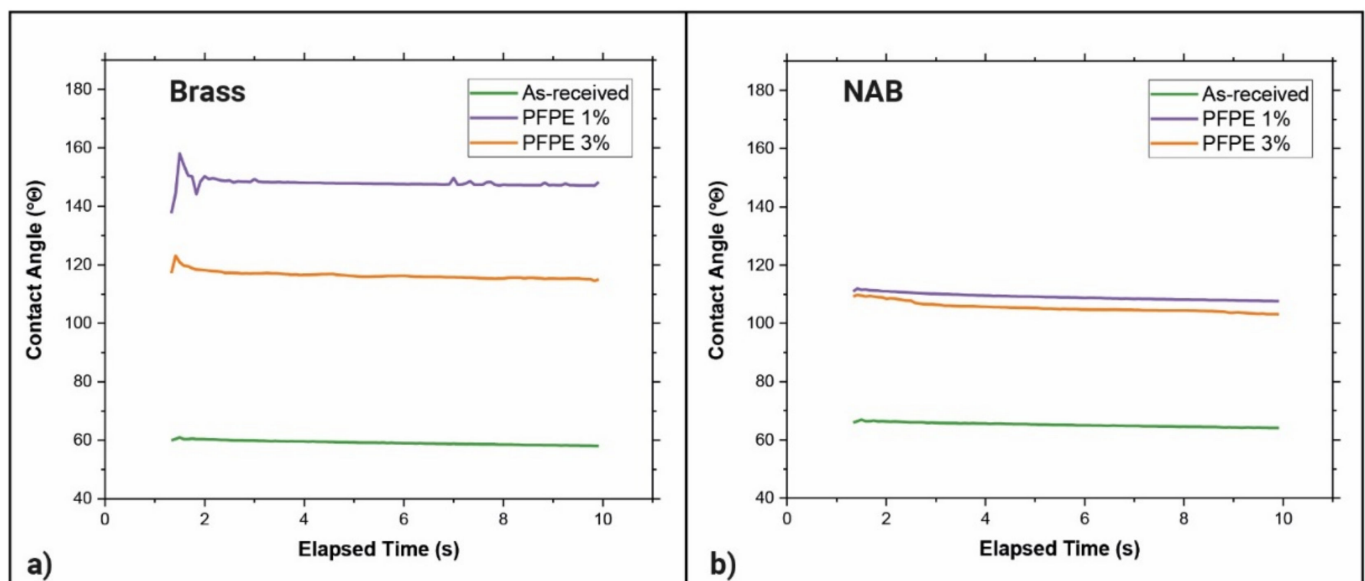

Figure 4. Contact angle as a function of time and coating typology.

The variation of the contact angle may indicate a coating excess or its weak bonding to the substrate surface. At the same time, a slight deviation from the initial contact angle (less than 2°) is standard and generally neglected, as also suggested by Yasuda et al. [34]. Therefore, the test was repeated five times, positioning the drop in different places on the surface to verify that the coating was evenly distributed. The maximum and minimum contact angles were recorded at 4 and 10 s, respectively, and their difference was averaged. The final results are shown in Table 4.

Table 4. Modification of the contact angle during time as an index of coating stability.

Substrates	As-Received	PFPE 1%	PFPE 3%
Brass	1.7 ± 0.9	1.3 ± 0.7	5.9 ± 0.8
NAB	2.3 ± 0.4	1.7 ± 0.7	7.2 ± 0.3

Although all the results always show values above 90°, the contact angle variations for PFPE 3% are always more significant than PFPE 1%, suggesting that the latter is more stable. These stronger contact angle variations depend on the fact that one or both the PFPE terminations are not bonded to the substrate. These terminations are polar and cause the drop to spread onto the surface due to a surfactant effect and, thus, lower contact angles are formed.

3.3. Corrosion of Un-Coated Samples

Figure 5 shows the corrosion process in the investigated time range due to the salt spray test. The brass with no coating shows progressively more intense corrosion. The process becomes evident starting from 6 h. Similarly, the NAB also corrodes significantly after 6 h.

Figure 5. Uncoated samples exposed to the salt spray harsh environment. Both materials start to corrode after 6 h.

Figure 6 shows an in-depth investigation of the corrosion process and a chemical assessment of the byproducts formed. The sample observed after 48 h shows an evident buildup of corrosion residuals [35]. However, the layer is not continuous, as can be observed from the top view of Figure 6a. More information can be obtained observing the material cross-section in Figure 6b. The β phase acted as an anode and was preferentially corroded, leaving the α dendritic parts almost unaltered in accordance with the work of Nunez [36].

On the other hand, no pure copper area was found, indicating that dezincification was not the leading corrosive process. The observation of the cross-section allows for better appreciation of the overall process. A thin 2.5 μm layer is visible at the surface, which formed during the corrosion process and was caused by corrosion debris buildup. Below, ca. 25 μm of material shows a strong deterioration. As described above, β phase has a spongy appearance, indicating that corrosion preferentially took place within these areas, as also shown by Sherif [37].

Figure 6c shows the EDS analysis performed in different sample locations. EDS measurements were performed on the material core before any exposure test and were used as a reference (blue line). The black line refers to the analysis performed on the exposed sample. In this case, high oxygen content was measured. The red line (cross-Section 1) refers to the outmost layer of the material. The EDS indicated a lower zinc content with respect to the base material, which could be interpreted as an initial dezincification process. This fact was also confirmed by observing the cross-section with an optical microscope, where a few brighter areas were observable. On the other hand, the green line (cross-Section 2) refers to an inner layer; thus, the results are practically indistinguishable from raw material.
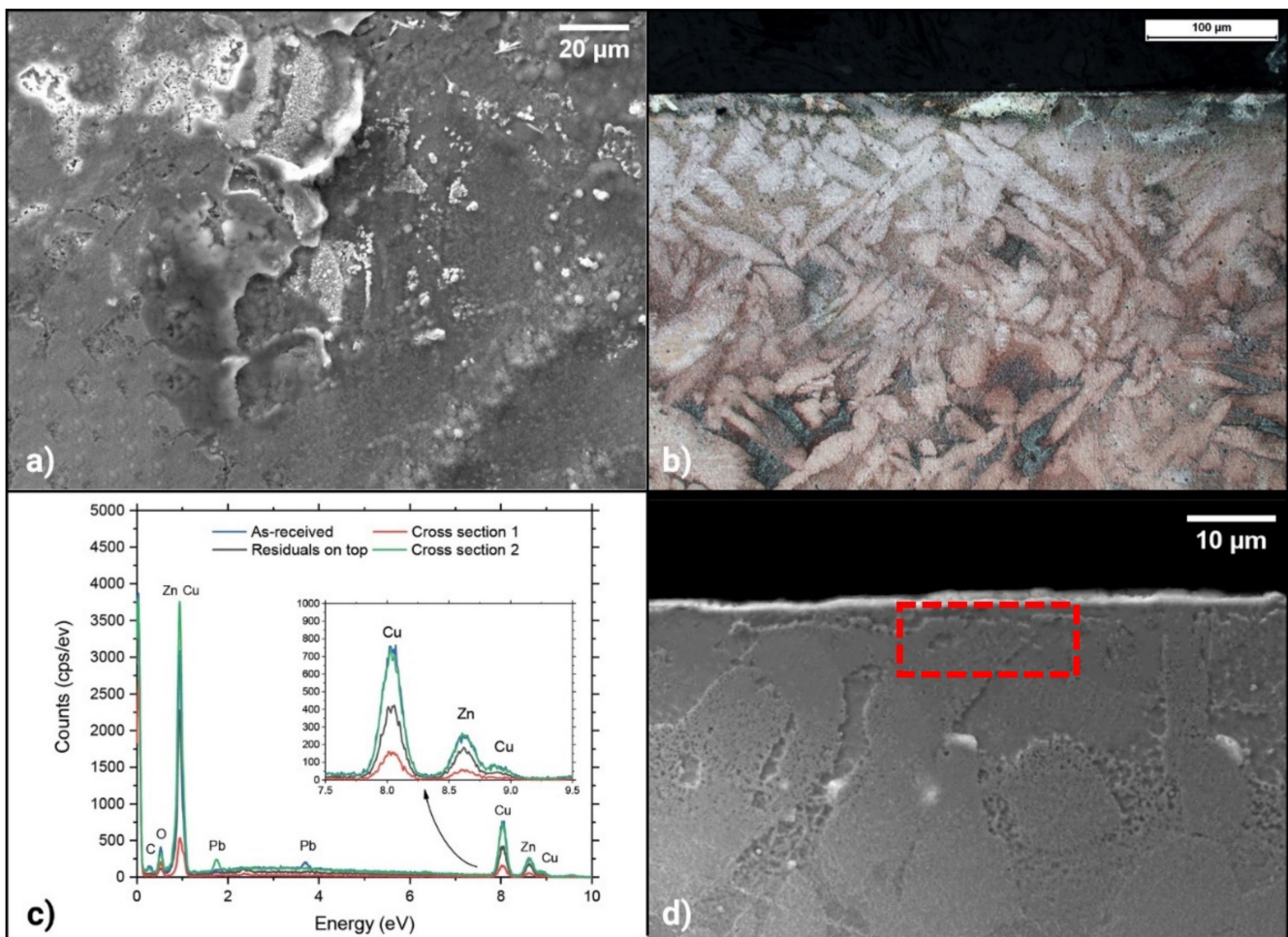
Figure 6. Brass sample after 48 h of exposure in a salt spray chamber. Sample observed from the top in the SEM (**a**), a cross-section of the same sample observed with an optical microscope in color (for evidencing dezincification) (**b**); EDS results obtained in different locations (**c**) and cross-section of the same sample at higher magnification (**d**). A red rectangle indicates where most of the EDS analysis was performed.

Similar to the previous case, Figure 7 shows the corrosion process of the NAB. Again, the top view shows a sponge-like surface, indicating that oxidation occurred, as also testified by the EDS (Figure 7a,c). In this case, the thickness of the corrosion debris is higher than in the previous case. The aggregates can be found as flat scales or arranged in circles, probably due to water drop evaporation, as also proposed by Stoffyn et al. [38]. Where the debris layer was not formed, it is still possible to see an unaltered α phase (acicular), while β was consumed. At the same time, dezincification and the formation of pure-copper areas are clearly visible in Figure 7b. The EDS analysis on the top of the sample (red line) indicated a substantial depletion in copper content. At the same time, the oxygen level increased, indicating the formation of an oxide layer. Furthermore, the comparison of the compositions in the cross-sections indicated that aluminum was the principally depleted element from the superficial layer, in accordance with the literature [39]. Figure 7d shows the thickness of the compound layer, which ranges between 5 and 9 μm.

3.4. Corrosion of Coated Samples

The coated samples were observed after exposure in the salt spray chamber after 1, 2, 6, 8, 24, and 48 h. Figure 8 shows the direct comparison of the brass samples with both the polymeric coatings.
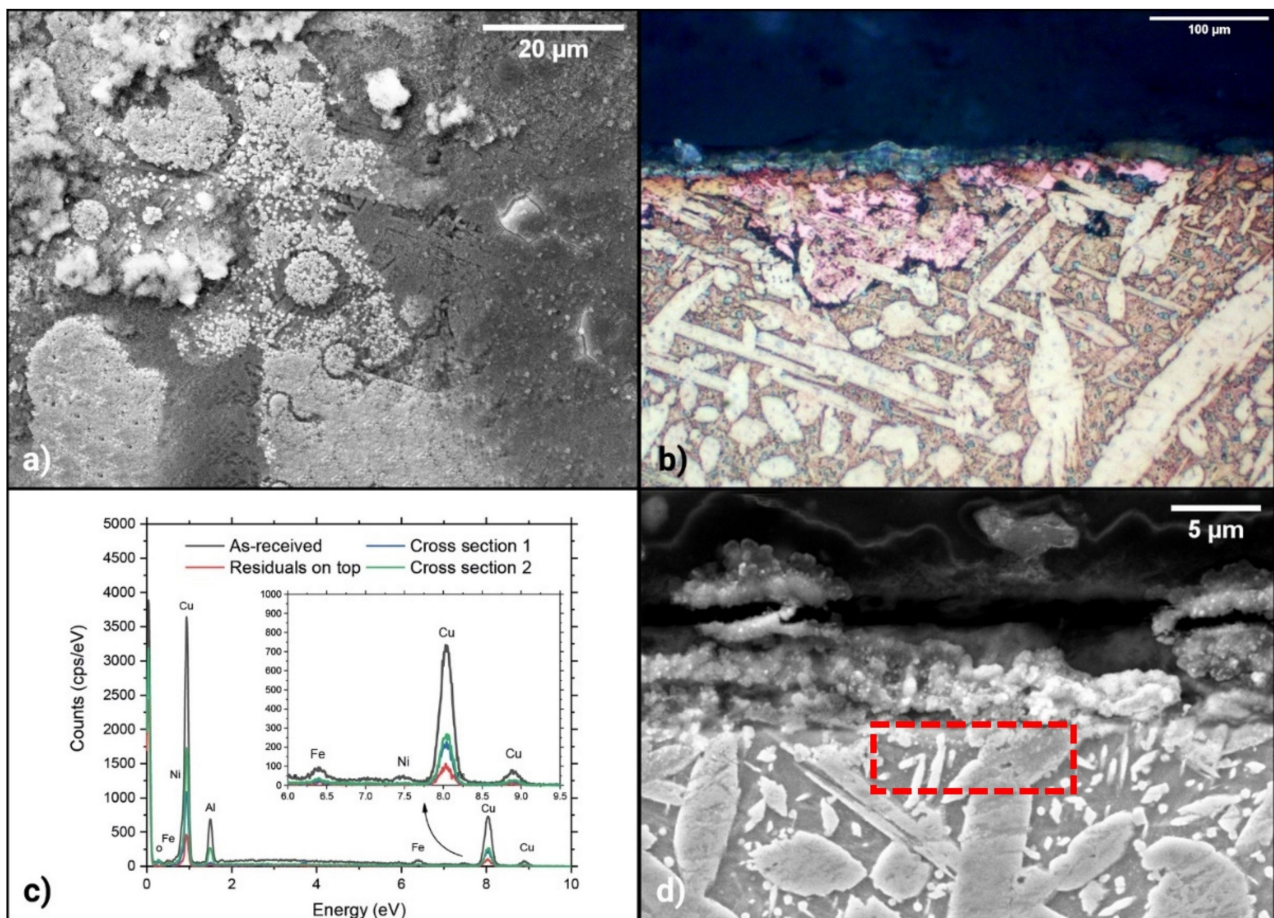
Figure 7. NAB sample after 48 h of exposure in a salt spray chamber. Sample observed from the top in the SEM (**a**), a cross-section of the same sample observed with an optical microscope in color, evidencing any preferential dealloying process (**b**); EDS results obtained in different locations (**c**) and cross-section of the same sample at higher magnification (**d**). A red rectangle indicates where most of the EDS analysis was performed.

Figure 8. Coated brass samples with two different coatings. PFPE 1% was more effective in preventing corrosion damages.

Figure 8 clearly shows how the coating differently protects the metallic substrate. The samples coated with the PFPE 1% acquire a matte surface after 6 h and slowly burnish in the last 48 h. It is worth noting that no corrosion buildup can be observed. Conversely, the brass coated with the PTFE 3% began to corrode after 6 h, the same as for the uncoated samples. A longer exposure time leads to large areas where the material is evidently corroded with pink coloration, suggesting that a large material portion underwent strong dezincification. A hypothesis to explain this harsher corrosion is that the polymer coating was not adherent to the substrate, and salty water could infiltrate it, leading to a mixed corrosion process where dezincification was assisted by differential aeration corrosion, as also proposed by Schneller et al. [40].

Figure 9 shows the brass sample observed with the SEM in the top view and cross-section.
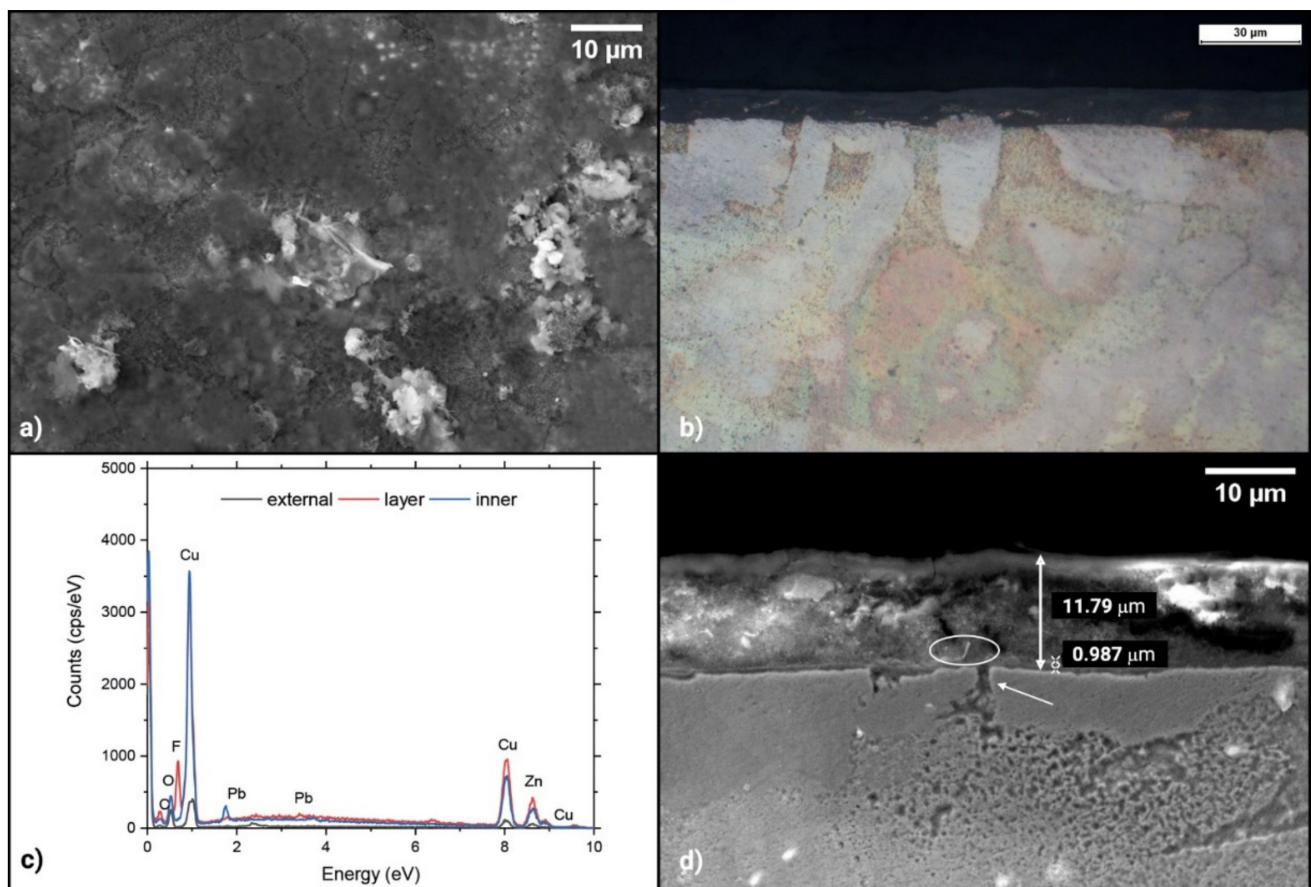

Figure 9. Brass coated with PFPE 1% sample after 48 h exposure in a salt spray chamber. Sample observed from the top in the SEM (**a**), a cross-section of the same sample observed with an optical microscope in color (for evidencing dezincification) (**b**); EDS results obtained in different locations (**c**) and cross-section of the same sample at higher magnification (**d**).

Figure 9a shows a homogeneous layer with only a few corrosion debris on the top, indicating less intense corrosion progress. This impression is confirmed by Figure 9b,d showing the sample in the cross-section. The optical microscope does not show pure copper zones, indicating that dezincification did not occur. Further information can be obtained using the SEM where the coating layer is still visible and ca. 1 μm thick. The picture shows a point where the interruption of the coating leads to the formation of a small pit. It is worth noting that the continuous layer generated above the protective layer is 12 ± 6 μm, like that formed on the uncoated sample, but the material altered below is thinner, ca. 10 μm, and evidenced only where the coating is interrupted. The EDS analysis in Figure 9c indicates a strong F peak in correspondence with the protective layer, confirming its presence even

after 48 h in a harsh environment. A stronger oxygen peak was found towards the outer part of the cross-section, while the inner part shows almost the same chemical composition as the as-polished material. Moreover, the lower number of debris attached to the material makes the overall surface look aesthetically better than the uncoated one.

Following the previous results related to the contact angle and its stability, the PFPE 3% was demonstrated as being significantly less effective in preventing the brass substrate from corroding. For these reasons, this coating was no longer investigated.

Figure 10 shows a similar test plan investigating the NAB substrate. Figure 10 shows a worse interaction between the PFPE and the substrate. Nevertheless, as for the brass, a higher polymeric concentration leads to a worse performance. This time, corrosion appears evident after 24 h for PTFE 1%, while 8h is enough for considerable surface damage when PTFE 3% is applied. In addition, the coating layer application leads to a slight color change that must be kept into account if aesthetic parameters are a concern. Moreover, in this case, the latter coating was no longer investigated due to its lower protective performance.
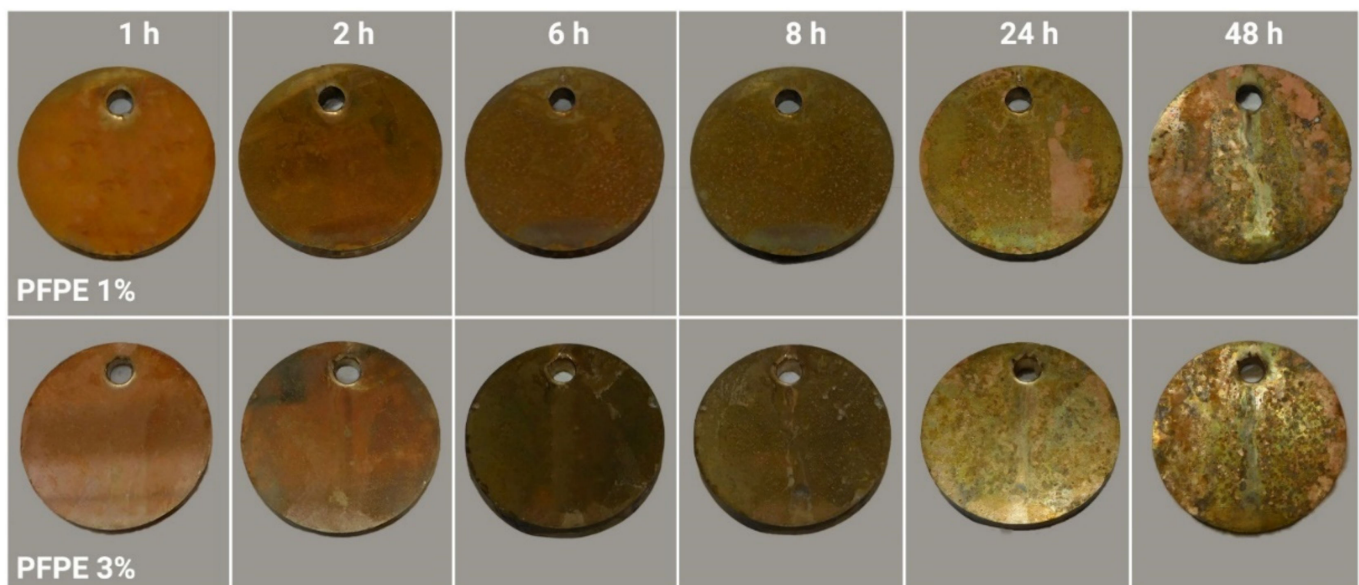

Figure 10. Coated NAB samples with two different coatings. PFPE 1% was also more effective in preventing corrosion damages in this case.

Figure 11 shows the NAB in its cross-section. In this case, the top view in Figure 11a and the inset show selective corrosion. The β phase is consumed, similar to what was observed for the uncoated material. Figure 11b shows a small portion of pure copper, which formed after selective dissolution and aluminum oxide formation. In this case, the compound layer formed is slightly thicker than the brass. The protective layer is often interrupted, explaining why the substrate corrodes more quickly. Moving towards the surface, the content of oxygen and aluminum increases, indicating that the aluminum oxide layer has formed. When deeper layers of the cross-section of the material are observed, the EDS shows a chemical composition closer to that of the as-received material. For a longer exposure time, i.e., 24 and 48 h, the NAB shows similar behavior to the brass, and a significant material portion assumes a reddish coloring, suggesting the harsh dealloying of the metal.
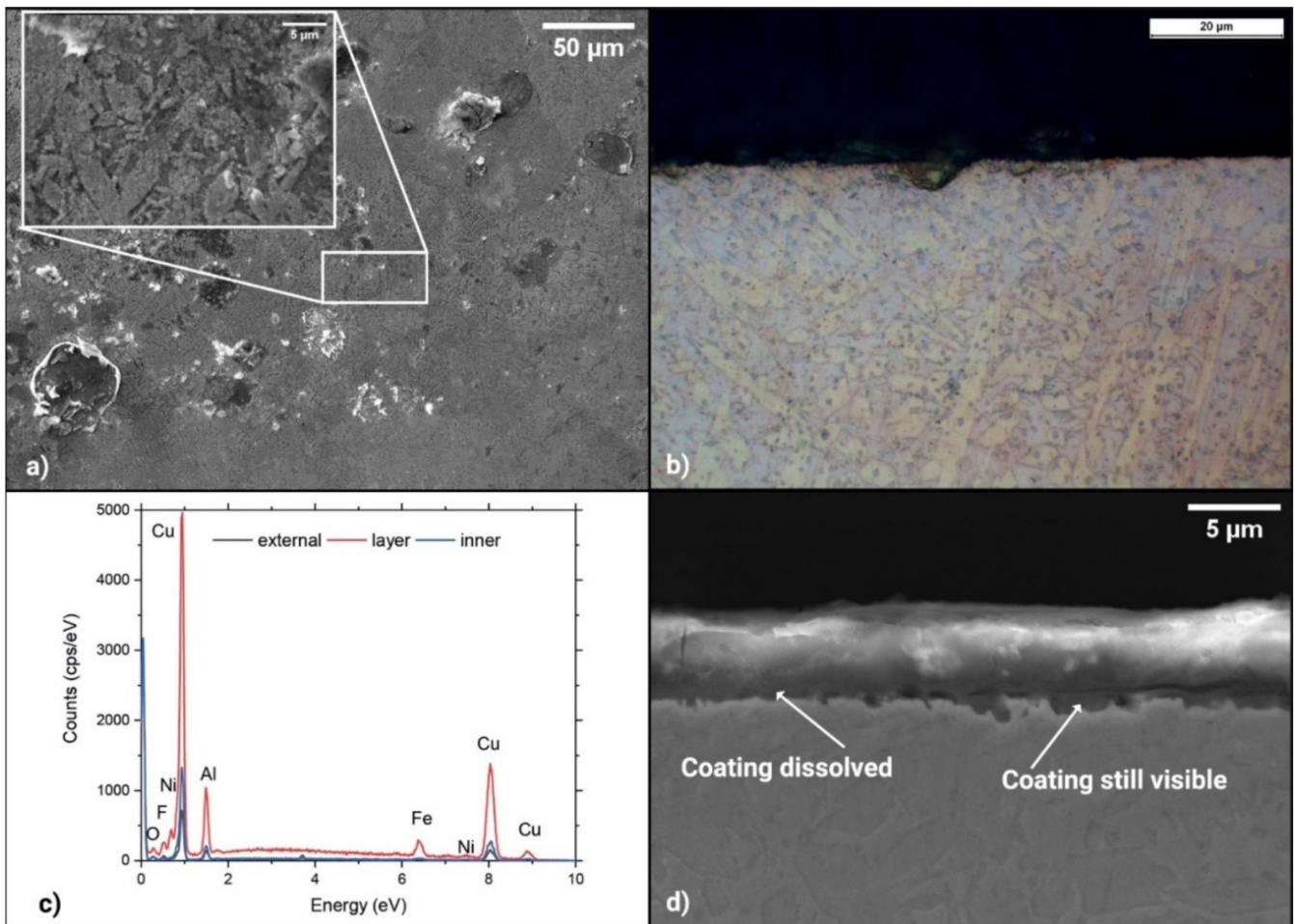
Figure 11. NAB coated with PFPE 1% sample after 48 h of exposure in a salt spray chamber. Sample observed from the top in the SEM (**a**), a cross-section of the same sample observed with an optical microscope in color (for evidencing dezincification) (**b**); EDS results obtained in different locations (**c**) and cross-section of the same sample at higher magnification (**d**).

4. Discussion

According to the experimental campaign, it is possible to affirm that brass has a higher affinity with the protective coating. The dip-coating leads to a less effective protective layer if the polymer has a higher concentration. This fact may be explained considering that a higher number of polymeric chains may impede the correct adhesion of the coating to the metallic surface. The lower adhesion between the metallic surface and the coating could lead to water and chlorides penetrating the barrier, speeding up the corrosion process. On the other hand, it must be considered that even in good adhesion conditions, a minor interruption of the coating continuity may lead to the onset of pitting corrosion, which is known for its complex recognition and could lead to the unexpected failure of components. Brass contains metallic lead particles, but their presence apparently did not affect the alloy's corrosion resistance.

Conversely, the NAB also showed lower corrosion resistance in the as-polished condition, and this could probably be related to the high iron content, which increases hardness but harms corrosion. Moreover, no specific heat treatment was performed to homogenize the material. The two substrates had similar surface finishing and, thus, the core reason for the worse adhesion and protective effect lies in the chemical composition of the alloy. Similar to the previous case, a higher polymer concentration in the dip-coating emulsion produces worse results and very fast corrosion rates compared to the uncoated samples.

5. Conclusions

This paper investigated the possibility of applying a PFPE layer to copper-based alloys via dip-coating. The adopted technique was effective in depositing the polymeric coating, since fluorine was still detected by EDS even after 48 h within the harsh environment produced by the salt spray chamber. The obtained coatings always have a similar thickness (ca. 900 nm) that is independent of the polymer concentration and which is maintained, unaltered, throughout the exposure test in the salt spray chamber. It is worth nothing that brass always provided higher contact angles than the NAB (155° vs. 110°). However, the coating application did not protect the substrates in the same way.

The following main conclusions can be drawn:

1. Lower polymer concentration in the dip-coating emulsion always leads to better adhesion of the coating to the substrates, hence, leading to higher protection and a slower corrosion process. Brass showed evident corrosion signs after 6 h when protected with the PFPE 3%; conversely, PFPE 1% allows a surviving time of 24 h without evident sign of corrosion. Similarly, NAB remains protected for only 2 or 6 h with PFPE 3% and PFPE 1%, respectively.
2. Brass can be effectively protected by PFPE 1% coating, but a slight change in the material coloration must be taken into account.
3. NAB is poorly protected by PFPE, irrespective of the polymer concentration of the coating emulsion chosen. This is particularly true when PFPE 3% is used, which shows corrosion signs after only 2 h.

References

1. Martini, G.; Ottaviani, M.F.; Ristori, S.; Lenti, D.; Sanguineti, A. Aggregation of Perfluorinated Polymers in Aqueous Solution Studied by ESR. *Colloids Surf.* **1990**, *45*, 177–184. [CrossRef]
2. Marchionni, G.; Ajroldi, G.; Pezzin, G. Molecular Weight Dependence of Some Rheological and Thermal Properties of Perfluoropolyethers. *Eur. Polym. J.* **1988**, *24*, 1211–1216. [CrossRef]
3. Chittofrati, A.; Lenti, D.; Sanguineti, A.; Visca, M.; Gambi, C.; Senatra, D.; Zhen, Z. Perfluorinated Surfactants at the Perfluoropolyether-Water Interface. *Colloids Surf.* **1989**, *41*, 45–59. [CrossRef]
4. Monduzzi, M.; Chittofrati, A.; Visca, M. Perfluoropolyether Water/Oil Microemulsions: A H NMR Self-Diffusion Study of Water. *Langmuir* **1992**, *8*, 1278–1284. [CrossRef]
5. Oldani, V.; del Negro, R.; Bianchi, C.L.; Suriano, R.; Turri, S.; Pirola, C.; Sacchi, B. Surface Properties and Anti-Fouling Assessment of Coatings Obtained from Perfluoropolyethers and Ceramic Oxides Nanopowders Deposited on Stainless Steel. *J. Fluor. Chem.* **2015**, *180*, 7–14. [CrossRef]
6. Ye, Z.; Chen, Y.; Yang, X.; Hu, W.; Ye, H. Development of Perfluoropolyether Modified Raspberry Paticles with Fine Hierarchical Structure and Their Application in Superhydrophobic Surface. *Colloids Surf. A Physicochem. Eng. Asp.* **2017**, *514*, 251–259. [CrossRef]
7. Sansotera, M.; Navarrini, W.; Gola, M.; Dotelli, G.; Stampino, P.G.; Bianchi, C.L. Conductivity and Superhydrophobic Effect on PFPE-Modified Porous Carbonaceous Materials. *Int. J. Hydrog. Energy* **2012**, *37*, 6277–6284. [CrossRef]

8. Gola, M.; Sansotera, M.; Navarrini, W.; Bianchi, C.L.; Gallo Stampino, P.; Latorrata, S.; Dotelli, G. Perfluoropolyether-Functionalized Gas Diffusion Layers for Proton Exchange Membrane Fuel Cells. *J. Power Source* **2014**, *258*, 351–355. [CrossRef]

9. Sansotera, M.; Bianchi, C.L.; Lecardi, G.; Marchionni, G.; Metrangolo, P.; Resnati, G.; Navarrini, W. Highly Hydrophobic Carbon Black Obtained by Covalent Linkage of Perfluorocarbon and Perfluoropolyether Chains on the Carbon Surface. *Chem. Mater.* **2009**, *21*, 4498–4504. [CrossRef]

10. Talaeemashhadi, S.; Sansotera, M.; Gambarotti, C.; Famulari, A.; Bianchi, C.L.; Antonio Guarda, P.; Navarrini, W. Functionalization of Multi-Walled Carbon Nanotubes with Perfluoropolyether Peroxide to Produce Superhydrophobic Properties. *Carbon* **2013**, *59*, 150–159. [CrossRef]

11. Marchese, G.; Bassini, E.; Parizia, S.; Manfredi, D.; Ugues, D.; Lombardi, M.; Fino, P.; Biamino, S. Role of the Chemical Homogenization on the Microstructural and Mechanical Evolution of Prolonged Heat-Treated Laser Powder Bed Fused Inconel 625. *Mater. Sci. Eng. A* **2020**, *796*, 14007. [CrossRef]

12. Bassini, E.; Vola, V.; Lorusso, M.; Ghisleni, R.; Lombardi, M.; Biamino, S.; Ugues, D.; Vallillo, G.; Picqué, B. Net Shape HIPping of Ni-Superalloy: Study of the Interface between the Capsule and the Alloy. *Mater. Sci. Eng. A* **2017**, *695*, 55–65. [CrossRef]

13. Wharton, J.A.; Barik, R.C.; Kear, G.; Wood, R.J.K.; Stokes, K.R.; Walsh, F.C. The Corrosion of Nickel-Aluminium Bronze in Seawater. *Corros. Sci.* **2005**, *47*, 3336–3367. [CrossRef]

14. Kenworthy, L.; O'Driscoll, W.G. Dezincification of Brasses. *Anti-Corros. Methods Mater.* **1955**, *2*, 247–249. [CrossRef]

15. Davies, D.D. *A Note on the Dezincification of Brass and the Inhibiting Effect OF Elemental Additions*; Copper Development Association Inc.: New York, NY, USA, 1993.

16. Lorimer, G.W.; Hasan, F.; Iqbal, J.; Ridley, N. Observation of Microstructure and Corrosion Behaviour of Some Aluminium Bronzes. *Br. Corros. J.* **1986**, *21*, 244–248. [CrossRef]

17. Krogstad, H.N.; Johnsen, R. Corrosion Properties of Nickel-Aluminium Bronze in Natural Seawater—Effect of Galvanic Coupling to UNS S31603. *Corros. Sci.* **2017**, *121*, 43–56. [CrossRef]

18. Wu, Z.; Cheng, Y.F.; Liu, L.; Lv, W.; Hu, W. Effect of Heat Treatment on Microstructure Evolution and Erosion-Corrosion Behavior of a Nickel-Aluminum Bronze Alloy in Chloride Solution. *Corros. Sci.* **2015**, *98*, 260–270. [CrossRef]

19. Tao, S.; Zhang, C.; Zhang, J.; Jiao, Y.; Li, M.; Lin, W.; Ran, L.; Clement, B.; Lyu, M.; Gentle, I.; et al. A Hydrophobic and Fluorophilic Coating Layer for Stable and Reversible Aqueous Zinc Metal Anodes. *Chem. Eng. J.* **2022**, *446*, 136607. [CrossRef]

20. Schröder, S.; Ababii, N.; Lupan, O.; Drewes, J.; Magariu, N.; Krüger, H.; Strunskus, T.; Adelung, R.; Hansen, S.; Faupel, F. Sensing Performance of CuO/Cu2O/ZnO:Fe Heterostructure Coated with Thermally Stable Ultrathin Hydrophobic PV3D3 Polymer Layer for Battery Application. *Mater. Today Chem.* **2022**, *23*, 100642. [CrossRef]

21. Wang, J.; Hu, H.; Zhang, J.; Li, L.; Jia, L.; Guan, Q.; Hu, H.; Liu, H.; Jia, Y.; Zhuang, Q.; et al. Hydrophobic Lithium Diffusion-Accelerating Layers Enables Long-Life Moisture-Resistant Metallic Lithium Anodes in Practical Harsh Environments. *Energy Storage Mater.* **2022**, *52*, 210–219. [CrossRef]

22. Nardi, J.A.; Strauss, J.A.; Fardo, F.M.; Ferreira, L.C.; Martini, E.M.A.; Horowitz, F. Wettability and Anticorrosion of Thin PTFE-like/Alumina Coatings on Carbon Steel. *Prog. Org. Coat.* **2020**, *148*, 105823. [CrossRef]

23. Xu, K.; Sun, W.; Wang, L.; Yang, Z.; Li, B.; Ma, Y.; Zhao, L.; Zhang, C.; Ma, S.; Han, H.; et al. Corrosion Protection Properties of Janus PTFE Coatings in Highly Corrosive H2SO4 Solutions. *Corros. Sci.* **2022**, *207*, 110553. [CrossRef]

24. Eshaghi, A.; Mesbahi, M.; Aghaei, A.A. Transparent Hierarchical Micro-Nano Structure PTFE-SiO2 Nanocomposite Thin Film with Superhydrophobic, Self-Cleaning and Anti-Icing Properties. *Optik* **2021**, *241*, 166967. [CrossRef]

25. Lin, L.; Emrich, S.; Kopnarski, M.; Schlarb, A.K. Lubrication Performance of a Polyetheretherketone (PEEK) and Polytetrafluoroethylene (PTFE) Blend within a Steel/Steel Tribosystem. *Wear* **2021**, *484–485*, 203997. [CrossRef]

26. Zhang, B.; Xu, W.; Zhu, Q.; Guan, F.; Zhang, Y. Nepenthes Pitcher-Inspired Lubricant-Infused Slippery Surface with Superior Anti-Corrosion Durability, Hot Water Repellency and Scratch Resistance. *J. Ind. Eng. Chem.* **2022**, *107*, 259–267. [CrossRef]

27. Sianesi, D.; Zamboni, V.; Fontanelli, R.; Binaghi, M. Perfluoropolyethers: Their Physical Properties and Behaviour at High and Low Temperatures. *Wear* **1971**, *18*, 85–100. [CrossRef]

28. Bracco, G.; Holst, B. *Surface Science Techniques*; Springer: Berlin/Heidelberg, Germany, 2013; Volume 51. [CrossRef]

29. Oddy, A.; Scott, D.A. Metallography and Microstructure of Ancient and Historic Metals. *Stud. Conserv.* **1992**, *37*, 282. [CrossRef]

30. Pantazopoulos, G.; Vazdirvanidis, A. Characterization of the Microstructural Aspects of Machinable a-b Phase Brass. *Microsc. Anal.* **2008**, *22*, 13–16.

31. Wright, R.N. Relevant Aspects of Copper and Copper Alloy Metallurgy. In *Wire Technology*; Butterworth-Heinemann: Oxford, UK, 2016.

32. Richardson, I. *Guide to Nickel Aluminium Bronze for Engineers*; Copper Development Association: New York, NY, USA, 2016.

33. Konen, R.; Fintov, S. Copper and Copper Alloys: Casting, Classification and Characteristic Microstructures. In *Copper Alloys—Early Applications and Current Performance—Enhancing Processes*; Books on Demand: Norderstedt, Germany, 2012.

34. Yasuda, T.; Okuno, T.; Yasuda, H. Contact Angle of Water on Polymer Surfaces. *Langmuir* **1994**, *10*, 2435–2439. [CrossRef]

35. Srivastava, A.; Balasubramaniam, R. Microstructural Characterization of Copper Corrosion in Aqueous and Soil Environments. *Mater. Charact.* **2005**, *55*, 127–135. [CrossRef]

36. Núñez, L.; Reguera, E.; Corvo, F.; González, E.; Vazquez, C. Corrosion of Copper in Seawater and Its Aerosols in a Tropical Island. *Corros. Sci.* **2005**, *47*, 461–484. [CrossRef]

37. Sherif, E.S.M.; Erasmus, R.M.; Comins, J.D. Corrosion of Copper in Aerated Synthetic Sea Water Solutions and Its Inhibition by 3-Amino-1,2,4-Triazole. *J. Colloid Interface Sci.* **2007**, *309*, 470–477. [CrossRef]

38. Stoffyn-Egli, P.; Buckley, D.E.; Clyburne, J.A.C. Corrosion of Brass in a Marine Environment: Mineral Products and Their Relationship to Variable Oxidation and Reduction Conditions. *Appl. Geochem.* **1998**, *13*, 643–650. [CrossRef]

39. Luo, Q.; Qin, Z.; Wu, Z.; Shen, B.; Liu, L.; Hu, W. The Corrosion Behavior of Ni-Cu Gradient Layer on the Nickel Aluminum-Bronze (NAB) Alloy. *Corros. Sci.* **2018**, *138*, 8–19. [CrossRef]

40. Schneller, T.; Waser, R.; Kosec, M.; Payne, D. *Chemical Solution Deposition of Functional Oxide Thin Films*; Springer Science & Business Media: Berlin/Heidelberg, Germany, 2013; ISSN 9783211993118.